Landsat 8 thermal data to support urban management and planning in the climate change era: a case study in Torino area, NW Italy

T. Orusa, E. Borgogno Mondino

T. Orusa, E. Borgogno Mondino, "Landsat 8 thermal data to support urban management and planning in the climate change era: a case study in Torino area, NW Italy," Proc. SPIE 11157, Remote Sensing Technologies and Applications in Urban Environments IV, 111570O (2 October 2019); doi: 10.1117/12.2533110

SPIE.

Event: SPIE Remote Sensing, 2019, Strasbourg, France

Landsat 8 thermal data to support urban management and planning in the climate change era: a case study in Torino area (NW Italy)

T. Orusa[a], E. Borgogno Mondino[b]

[a]Green Office Climate Energy & Change Groups, University of Turin, Italy, [b]DISAFA – Department of Agriculture, Forest and Food Sciences of Torino University, L.go P. Braccini 2, Grugliasco, TO, Italy)

ABSTRACT

Land surface temperature (LST) is an important factor in global climate change, vegetation growth, and urban heat island (UHI). LST is one of the most important environmental variables measured by satellite remote sensing. Public domain data are available from the operational Landsat-8 Thermal Infrared Sensor (TIRS). The present study focuses on determining and mapping UHI for the metropolitan city of Turin in Piedmont Italy using Landsat 8 multitemporal collection dataset from 2013 to 2018. The main purpose of this research is to give an instrument for the present urban management and future urban planning in order to increase city resistance and resilience against climate change through mitigation and adaptation. Improving green areas using urban forestry can be a way to mitigate Summer heat waves and trying to regulate the high demand of energy for cooling buildings. LST has been estimated using the Radiative Transfer Equation (RTE) while the LSE (Land Surface Emissivity) according to the NDVI Thresholds Method. In the multitemporal collection the UHI has been detected after calculating zonal statistics. Surfaces with similar thermal behave have been mapped using an Unsupervised classification (K-means). Through the considered years, the analysis has revealed how UHI are very common and persistent in the metropolitan Turin area, where vegetation and water content are lower and where there are a high number of buildings in concrete and asphalt is widespread.

Keywords: Landsat 8 TIRS, LST, NDVI, UHI, mapping, mitigation, climate change, urban forestry.

INTRODUCTION

Land surface temperature (LST) is related to surface energy and water balance, at local through global scales, with principal significance for a wide variety of applications, such as climate change, urban climate, the hydrological cycle, and vegetation monitoring [1–4]. For these reasons LST represents one of the key climate variables retrievable from space-based remote sensing platforms, offering insight into a range of environmental processes and linking multiple disciplines across the natural and physical sciences. Apart from being a fundamental variable in quantifying elements of the surface energy budget [5], LST has been used to study ocean–atmosphere interactions [6], to track global warming and climate change impacts [4,7], as well as being widely used in studies of vegetation monitoring [8], drought persistence [9] and urban climate assessments [10]. LST also plays a critical role in linking the water and energy cycles through its relationship with surface heat fluxes [11]. Indeed, thermal infrared (TIR) observations represent a fundamental element in efforts to map the spatial distribution of evaporation [12] as well as in efforts to constrain land surface model simulations [13]. Given the role that LST plays across broad aspects of earth and environmental sciences, determining its spatial and temporal variability is of considerable interest [14]. However, accurately determining its absolute value, in addition to describing its spatial and temporal development, is challenging given that LST varies considerably throughout the diurnal cycle as a function of the surface radiative balance, as well as expressing a broad range of spatial and temporal variations due to changing land surface and atmospheric conditions [15,16]. The urban heat island (UHI) effect is a phenomenon that the land surface temperature in urban areas is apparently higher than that in rural areas [17]. The causes of UHI are diverse, including natural factors and human factors, whose root cause is the change of land use. Additionally, the factors such as urban configuration, heat release from anthropogenic heat source, atmospheric pollution, geographic location, and climate also affect the UHI [18]. With the development of urbanization, urban built-up areas, namely, impervious surfaces,

Remote Sensing Technologies and Applications in Urban Environments IV, edited by Thilo Erbertseder, Nektarios Chrysoulakis, Ying Zhang, Proc. of SPIE Vol. 11157, 111570O · © 2019 SPIE
CCC code: 0277-786X/19/$21 · doi: 10.1117/12.2533110

including roads and buildings, instead of green lands and water bodies, are rapidly sprawling and, thus, the city will suffer from the UHI effect [19]. Shenzhen, a main financial center in Southern China, increased its urban areas from around 3.06% to 39.3% from 1986 to 2005 [20], Hong Kong is a metropolis with a high population density filled with high-rise buildings and has a lack of public open spaces in urban areas [21], therefore, the urban areas in Shenzhen and Hong Kong suffer from a severe UHI effect. The traditional method for UHI study relies on meteorology data derived from urban and rural weather stations. It is difficult to obtain abundant meteorology data and impossible to acquire surface meteorology data, aside from dotted meteorology data [22,23]. After the launch of the first artificial Earth satellite, Sputnik, in 1957, satellite images have been widely applied in various fields. The satellite images with a thermal infrared band, such as the images of Landsat TM, Landsat OLI-TIRS, ASTER (Advanced Spaceborne Thermal Emission and Reflection Radiometer) and MODIS (Moderate Resolution Imaging Spectroradiometer), can be converted to land surface temperature (LST) to study the UHI. In 1972, Rao firstly proposed that remote sensing could be applied to study the UHI and produced a land surface thermal distribution graph by the thermal infrared data from satellite images [24,25]. After that, satellite images have been widely used to study the LST and UHI. Therefore, various algorithms, such as the mono-window algorithm (MWA), single-channel method (SCM) and split-window algorithm (SWA) and Radiative Transfer Equation (RTE) were proposed for LST estimation. Howard firstly discovered the temperature in the center of London was obviously higher than that in its suburbs [26,27]. In China, the LST and land use classification were first applied in Guangzhou, China using the Landsat TM data from 1985 to 2000 to compare the correlation between the UHI and land use types, and suggested that the urban greening and landscape designs in Guangzhou should consider more about vegetation types, namely forest, shrubs, and lawns, to control the UHI [28]. In Canada, the temperature difference among different land use types in Toronto on 3 September 2008 using the Landsat TM data discovered that the higher urban utilization corresponded to higher UHI intensity [29].

In conclusion urban heat island (UHI) effect indicates the higher air and land surface temperature (LST) in urban areas in comparison to the surrounding rural area, generated by high levels of near-surface energy emission, solar radiation absorption of ground objects and low rates of evapotranspiration (with urban concentrations generating modelled and observed changes in regional temperatures [30]. The relationship between landscape pattern and UHI becomes globally considerable [31]. A large number of studies considered that the built-up area and bare land accelerate the effect of UHI, whereas green space and water reduce the UHI intensity [32]. Furthermore, LST is controlled by the complex pattern of landscape composition and configuration [33]. Some researchers have found that natural and socio-economic factors simultaneously create certain effects on LST pattern [33]. Landsat 5 TM and Landsat 8 OLI thermal infrared data with 120 and 100 m spatial resolutions, respectively, have been utilized for local-scale studies of UHI [34]. A variety of algorithms have been developed to retrieve LST from Landsat data, such as mono-window algorithm, single-channel algorithm [36], etc. Urban hot spots (UHS), the special urban thermal features, experience extreme heat stress mainly developed by man-made activities within a UHI zone [37]. So, identifying these UHS for mitigation purpose becomes an important task to maintain the ecological balance within a city. Different scholars in different time periods attempted to draw a correlation between LST in UHIs and some land use/land cover (LU–LC) indices for different study area [38]. Landsat-8 was successfully launched on 11 February 2013 and deployed into orbit with two instruments on-board: (1) the Operational Land Imager (OLI) with nine spectral bands in the visual (VIS), near infrared (NIR), and the shortwave infrared (SWIR) spectral regions, and (2) the Thermal Infrared Sensor (TIRS) with two spectral bands in the LWIR. The spatial resolution of TIRS data is 100 m (resampled at 60 m) with a revisit time of 16 days, and as a result, applications are different than those of other sensors with coarser spatial resolutions and shorter revisit times. In this paper, the main purpose is to give an instrument for the present urban management and future urban planning focusing on determining and mapping UHI for the metropolitan city of Turin in Piedmont Italy in order to increase resistance and resilience in the study area against climate change through mitigation and adaptation.

STUDY AREA

The metropolitan area of Turin is located in Piedmont, in the North West of Italy. In this case of study it has been analysed an area around 1000 km^2 including some of the following municipalities areas: Alpignano, Baldissero Torinese, Beinasco, Borgaro, Collegno, Druento, Gerbido, Grugliasco, Mappano, Moncalieri, Nichelino, Orbassano, Perosa, Pecetto, Pino torinese, Rivalta Torinese, Rivoli, San Mauro Torinese, Torino, Venaria etc…Turin is the capital city of Piedmont and it is one of the most important metropolitan city of Italy. It is located

in the Po river basin and it's surrounded by hills in the South and Alps in the North-West. The latitudinal and longitudinal of Turin is 45°04′ N 7°42′ E (WGS84). Geologically, Turin is characterized by Quaternary alluvial and lacustrine deposits. The city has an elevation of 200–715 m. The soil is mainly alluvial with clay minerals and organic matters with shallow water content. Turin's climate is classified as warm and temperate. Turin is a city with a significant rainfall. Even in the driest month there is a lot of rain. Turin is characterized by humid subtropical (Cfa) climate according to the Köppen-Geiger system classification [39]. Summer season is hot, while winter season is cool and moist. July and August are the hottest months, while December and January are the coldest months. The temperature of Turin often is lower to the other metropolitan areas of Piedmont due to the presence of prevailing wind from the nearer Val di Susa Valley. Rainfall is convectional (in Spring and Autumn). The mean annual temperature varies from -2.5°C to 27.9°C and average annual rainfall is about 850-1000 mm [World Meteorological Organisation (United Nations)]. The only area of Turin city is about 130.2 km^2. Turin experiences a very high density of population (6750.67 persons/km^2) [Italian National Institute of Statistics (Italian: Istituto Nazionale di Statistica; Istat)]. Tourism, manufacturing in particular cars, food and wine production are the dominant industries of Turin. The city is well known for Italian fashion hub and architectural heritage.

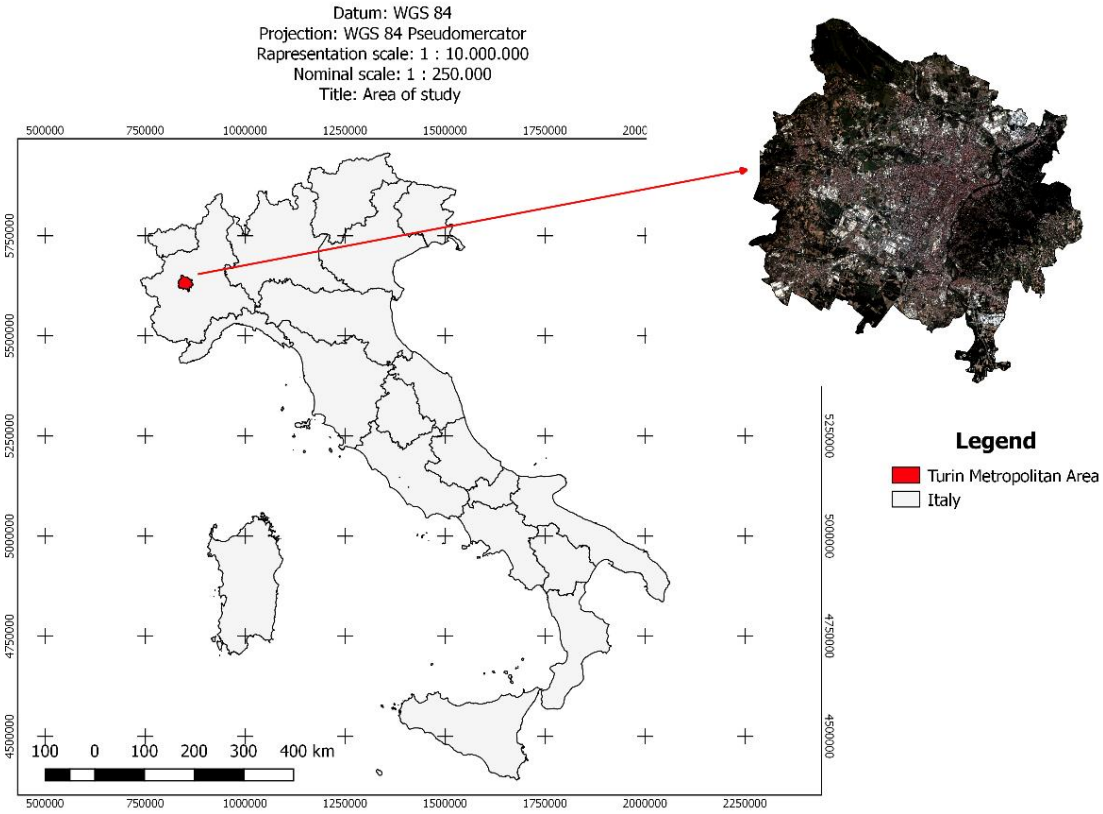

Figure 1 Area of study (Reference Frame: WGS84 UTM 32N)

MATERIALS AND METHODS

Materials

For this paper, it has been used USGS Landsat 8 Surface Reflectance Tier 1 Collection (LANDSAT/LC08/C01/T1_SR/LC08). Each scene has been downloaded from Google Earth Engine [40] clipped with the area of interest (AOI), a shape polygon of the metropolitan area of Turin. LST and NDVI were retrieved from the following bands: 4 Red {0.64 - 0.67 µm} with GSD 30 m; 5 Near-Infrared {0.85 - 0.88 µm} with GSD 30 m; 10 TIRS 1 {10.6 - 11.19 µm} with a GSD 100 m resampled at 60 m of the Landsat 8 OLI and TIRS images of the metropolitan area of Turin. The images collection used for this research including each EO Landsat 8 data acquired over Turin from from 11th April 2013 to 31th December 2018 for a total of six years of observation with a revist time of 16 days and acquisition times that corresponding at 10.13 ± 0.15 GMT. The total amount of scene is 237 images for each bands used including also the pixel quality dataset.

LST has been resampled at 30 m using the software tool SAGA GIS vers.9.0.0 [41]. USGS Landsat 8 Surface Reflectance Tier 1 Collection dataset is atmospherically corrected at surface reflectance. These images contain five visible and near-infrared (VNIR) bands and two short-wave infrared (SWIR) bands processed to orthorectified surface reflectance, and two thermal infrared (TIR) bands processed to orthorectified brightness temperature. These data have been atmospherically corrected by the provider using LaSRC [42] and includes a cloud, shadow, water and snow mask produced using CFMASK [42], as well as a per-pixel saturation mask. In order to calculate zonal statistics and create maps it has been used also the software QGIS vers. 2.18.00 [43] Even if LST cannot be assimilated to air temperature in order to evaluate LST calculation, it has been compared the air temperature with LST pixels in correspondence of meteorological stations in green areas and parks and also water basin where temperature is not affected to the high absorbance of manmade materials and rocks, and so it can be compared and validate with LST. The RMSE calculated during the processing for the entire filtered collection is 1.5°C. In this case of study the validation has been conducted using meteorological stations spread on the area of interest. In particular 10 meteorological stations have been considered, but only three has been used because the others are located in areas in which material physical properties do not permitted to link LST with surface air temperature (collected following WMO correct procedures).

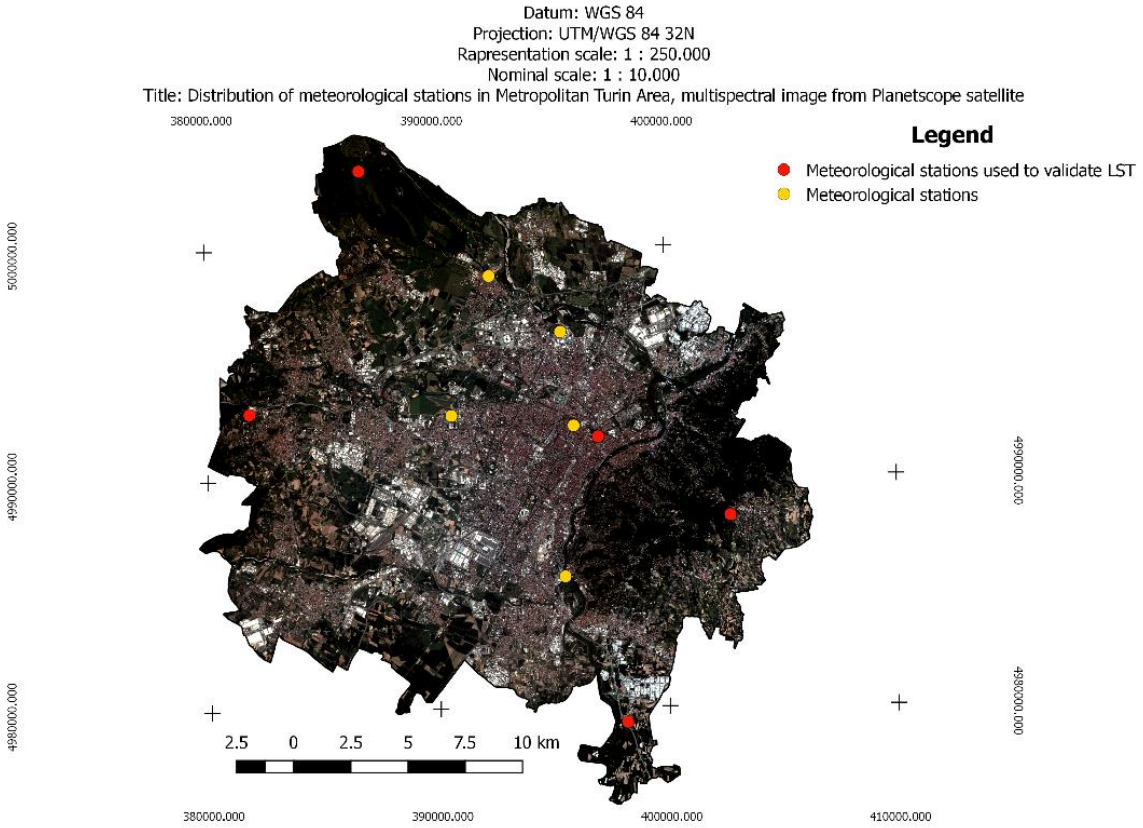

Meteorological station (ARPA Piemonte) http://www.arpa.piemonte.it/	UTM_X WGS84	UTM_Y WGS84
Baducchi	**398146**	**4979330**
Pino Torinese	**402746**	**4988284**
Rivoli	381856	4992919
Torino Alenia	390656	4992737
Torino Giardini Reali	**397030**	**4991748**
Torino Reiss Romoli	395447	4996309
Torino Vallere	395514	4985692
Torino Via della Consolata	395972	4992235
Venaria Ceronda	392378	4998772
Venaria La Mandria	**386790**	**5003396**

Fig 2 Meteorological stations distribution in the Metropolitan Turin area (Reference Frame: WGS84 UTM 32N)

Methods

The dataset USGS Landsat 8 Surface Reflectance Tier 1 Collection has been use to calculate LST and NDVI from band 4-5-10 of the Landsat 8 OLI and TIRS. The thermal infrared band (band 10) for Landsat 8 TIRS image has a spatial resolution of 100 m. This thermal band was resampled using the nearest neighbor algorithm [41] with a pixel size of 30 m to match the optical bands.

After creating a multitemporal stack in SAGA GIS [41] the bands 4-5 have been used to calculated NDVI as follow:

$$\mathrm{NDVI} = \frac{\mathrm{NIR\ (b5)} - \mathrm{RED\ (b4)}}{\mathrm{NIR\ (b5)} + \mathrm{RED(b4)}} \qquad (1)$$

LST was retrieved by Brightness temperature (in Kelvin) already present into the dataset collection. For Landsat 8 OLI, K_1 is 774.89 and K_2 is 1321.08.

The surface emissivity, **ε**, was estimated using the NDVI thresholds method [44; 45; 46; 47]. The fractional vegetation, Fv, of each pixel was determined from the NDVI using the following equation [48]:

$$F_v = \left(\frac{\mathrm{NDVI} - \mathrm{NDVI_{min}}}{\mathrm{NDVI_{max}} - \mathrm{NDVI_{min}}}\right)^2 \qquad (2)$$

where $NDVI_{min}$ is the minimum NDVI value (0.2) where pixels are considered as bare soil and $NDVI_{max}$ is the maximum NDVI value (0.5) where pixels are considered as healthy vegetation.

dε is the effect of the geometrical distribution of the natural surfaces and internal reflections. For heterogeneous and undulating surfaces, the value of dε may be 2% [48].

$$d\varepsilon = (1 - \varepsilon_s)(1 - F_v)F\varepsilon_v \qquad (3)$$

where ε_v is vegetation emissivity, ε_s is soil emissivity, F_v is fractional vegetation and F is a shape factor whose mean is 0.55 [44].

$$d\varepsilon = \varepsilon_v F_v + \varepsilon_s(1 - F_v) + d\varepsilon \qquad (4)$$

where ε is emissivity. From Equations (4) and (5), ε may be determined by the following equation:

$$\varepsilon = 0.004 * F_v + 0.986 \qquad (5)$$

With this equation Land Surface emissivities (LSE) has been calculated for all the multitemporal series of 6 years. LST in (°C) finally was derived for each image using the following equation [49]:

$$\mathrm{LST} = \frac{T_B}{1 + \left[\frac{\lambda \sigma T_B}{hc}\right] * \ln\varepsilon} - 273.15 \qquad (6)$$

where λ is the effective wavelength (10.9 the mean between 10.6 - 11.19 μm for band 10 in Landsat 8 data), σ is Boltzmann constant (1.38×10^{-23} J/K), h is Plank's constant (6.626×10^{-34} Js), c is the velocity of light in a vacuum (2.998×10^{-8} m/sec) and ε is emissivity.

LST collection has been filtered considering the pixel quality given by the EO Data provider using the software IDL ENVI vers. 8.0.0 with a selfmade script algorithm in order to obtain images without clouds [50]. Before starting this procedure the total images number of multitemporal series was 237 after the filtering 143, for a total overall observation of six years.

The LST filtered collection has been used to produce zonal statistics for each pixels through the multitemporal series using IDL software in particular: median (m), standard deviation (std) and m^{*std} where:

$$m^{std} = 3 * m - std \quad (7)$$

Median and m^{*std} obtained through the multitemporal series have been subjected to a cluster analysis in order to identify areas with similar behave in the SAGA GIS tool [41]. An Unsupervised automatic classification K-Means has been realized. It has been identify 8 clusters according to the method Minimum Distance and Hillclimbing combined [41] in order to map metropolitan Turin areas.

UHI and non-UHI were identified by the range of LST determined by the following equations [51] with a diffence instead of using mean in thic study it is used the median:

$$\mathrm{LST} = \mathrm{m} + 0.5 * \delta \quad (8)$$

$$0 < \mathrm{LST} \leq \mathrm{m} + 0.5 * \delta \quad (9)$$

where m and δ are the median and standard deviation of LST in the study area, respectively.

In this study, LST statistics maps were used in delineating the UHS in Turin to provide special emphasis for continuous monitoring. These UHS (Urban Hot Spot) were delineated by the following equation [52]:

$$\mathrm{LST} > \mathrm{m} + 2 * \delta \quad (10)$$

Statistics on meteorological data has been realized using the historical dataset of ARPA Piedmont, the Regional Agency for Environmental Proctection.

RESULTS

Before performing any kind of application process, a validation of derived LST is absolutely necessary with in situ measurement or with another type of satellite sensor for example MODIS. In the present research, in situ measurement data were used to validate the LST values as a reference tool. In order to test the good quality of thermal calibration processing each images of the filtered collection LST has been validated with the temperature detected by a some meteorological stations. Even if LST is different to air temperature to bypass this it has been considerd only the meteorological stations in non-anthropic areas such as buildings, roads etc with a natural area with a minimum extent of 10.000 m^2 (a pixel thermal Lansat 8). These particular meteo-stations shown in fig. 2 are located in green areas with a preminent cover in grass. The performed analysis considering the same time in the data acqusition by satellite and meteo-stations, show how in these natural areas LST differ from meteo station with a maximum of 1.00°C for all considered data. To sum up the table in fig.3 shows the LST and the air temperature of all seasons and the meteorological summer in the six years.

Meteorological station	LST (pixel meteo station) T(°C)	Meteo Station T (°C)	LST (pixel meteo station) T(°C)	Meteo Station T (°C)
Baducchi	29.3	28.08	10.8	9.46
Pino Torinese	25.5	24.74	8.4	9.16
Rivoli	30.0	28.55	10.1	10.60
Torino Giardini Reali	30.3	29.84	11.4	11.17
Venaria La Mandria	26.2	26.03	8.6	7.07
Mean	28.3	27.45	9.8	9.5
Standard Deviation	2.02	1.83	1.19	1.42

Fig.3 Valide LST

The decision to map LST median and m^{*std} through 6 yeas depending on the following reason: the median consider the LST and the UHI phenomenon during all the seasons while m^{*std} permitted in these anaylisis on focusing to the Meteorological Summer season (from June to August). The following maps produced permitted to observe how LST, UHI and UHS are distrubuted in Turin considering all the observation years. The cluster analysis considering 8 groups, has revealed areas with similar thermal behave as follow:

Cluster	Elements	Std.Dev.	LST (°C) all seasons
1	30938	0.36	12.9
2	65906	0.22	12.1
3	72140	0.21	11.4
4	71388	0.21	10.7
5	76341	0.20	10.0
6	86148	0.19	9.3
7	60708	0.23	8.6
8	33472	0.38	7.7

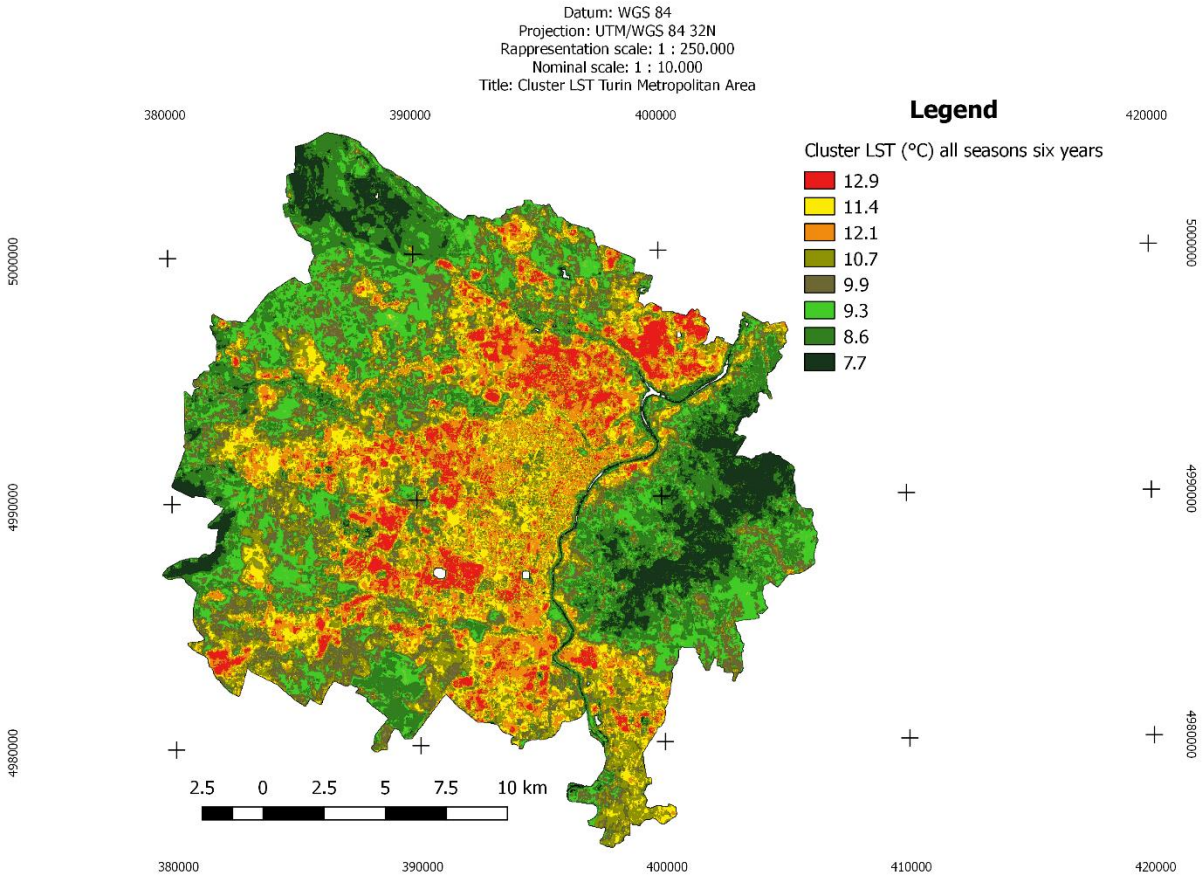

Fig.4 LST clusters all seasons considering six years and relative data table (Reference Frame: WGS84 UTM 32N)

Cluster	Elements	Std.Dev.	LST (°C) all seasons Meteorological Summer
1	6697	1.64	37.2
2	41028	0.63	34.0
3	74530	0.45	32.3
4	80843	0.42	30.8
5	89042	0.41	29.4
6	91474	0.41	28.0
7	67834	0.46	26.5
8	45593	0.67	24.8

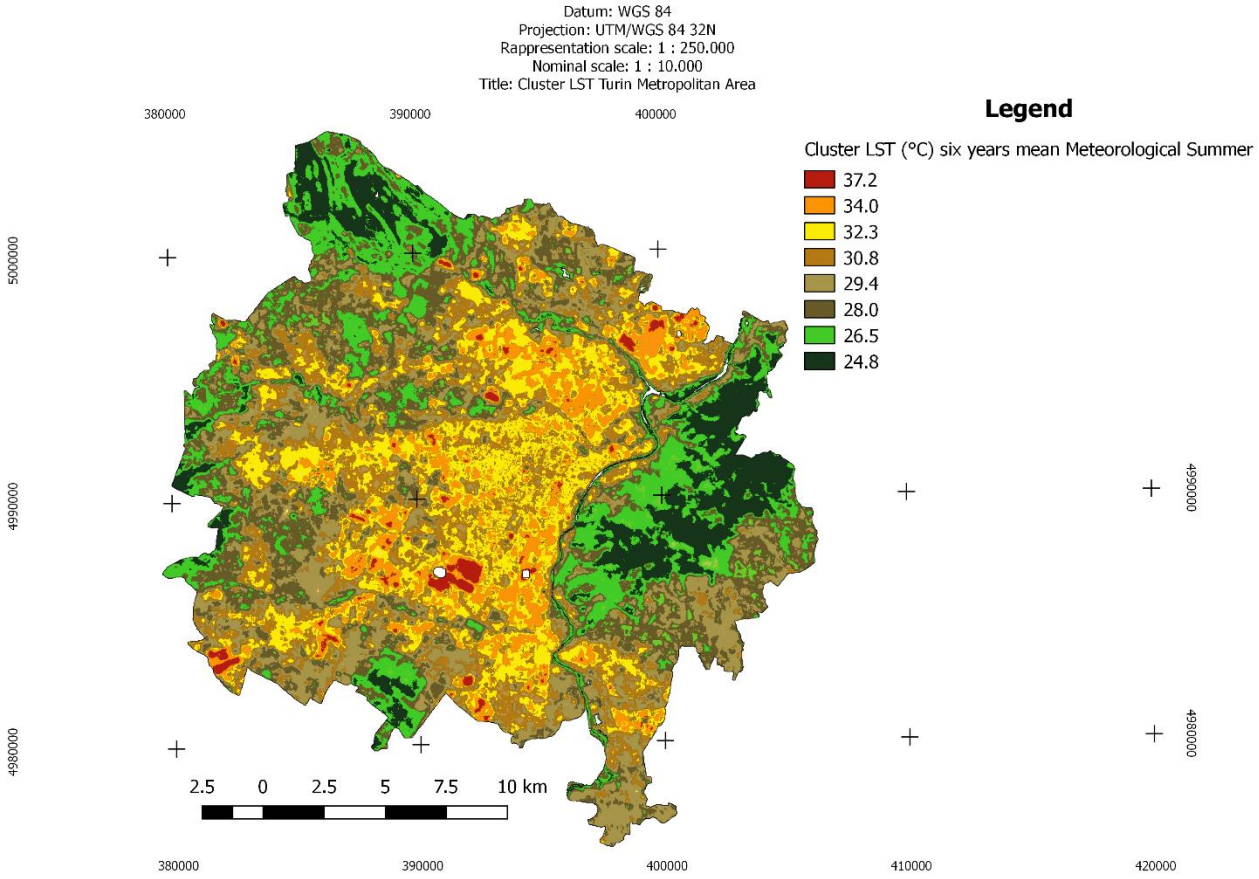

Fig.5 LST clusters meteorological summer seasons considering six years and relative data table (Reference Frame: WGS84 UTM 32N)

The intensity of UHI may be defined as the difference.between the average or median temperature of UHI and non UHI (according to formula 9). In Turin Metropolitan area, the UHI zones consistently extend from North-East to South especially around the city belt where factories and social housing districts are spread. It is interesting to see how natural park, tree-lined streets are able to reduce significantly the temperature in the area.

Cluster	Elements	Std.Dev.	UHI Mean temperature (°C) all seasons
1	33935	0.67	15.5
2	69389	0.40	14.0
3	78953	0.37	12.7
4	78012	0.37	11.4
5	84326	0.36	10.2
6	82854	0.36	9.0
7	52992	0.45	7.6
8	16580	0.88	5.6

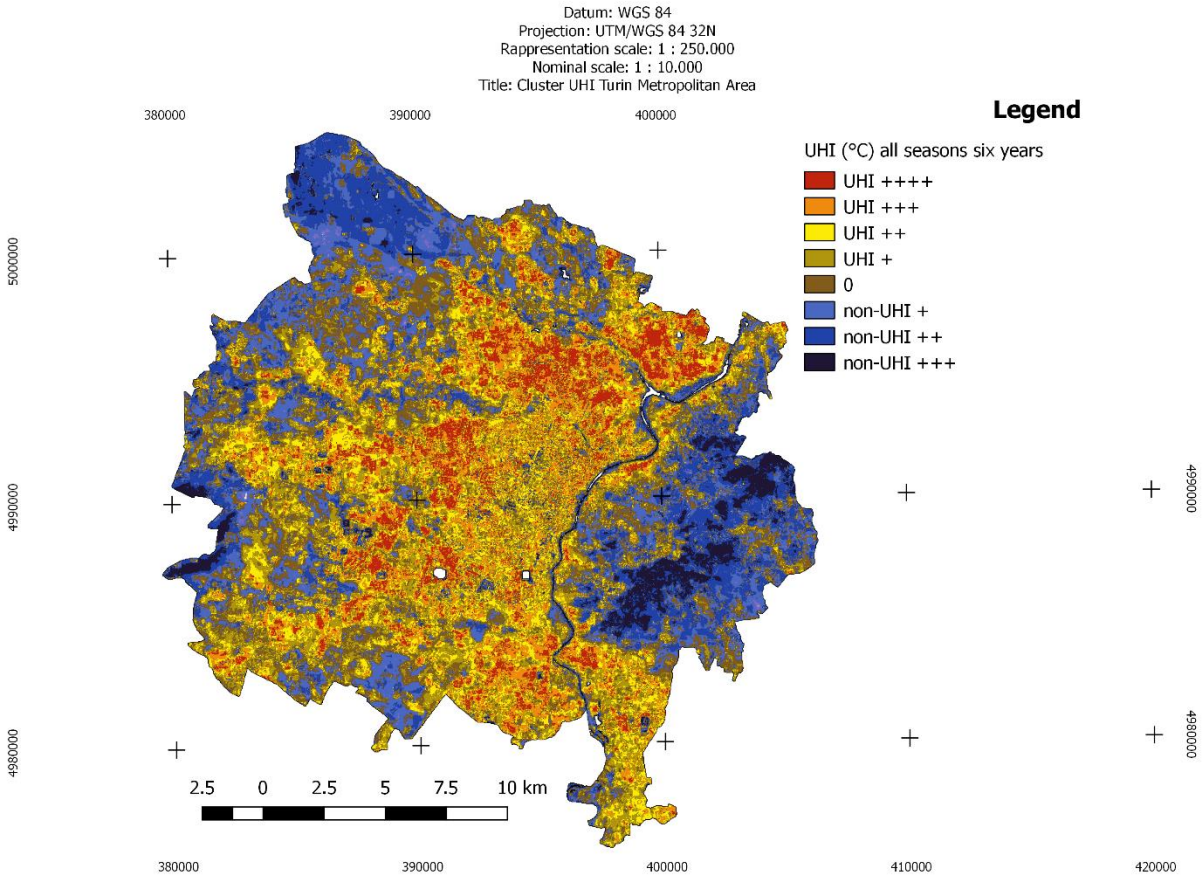

Fig.5 UHI clusters all seasons considering six years and relative data table (Reference Frame: WGS84 UTM 32N)

Cluster	Elements	Std.Dev.	UHI Mean temperature (°C) Meteorological Summer
1	20140	1.14	37.1
2	63136	0.56	34.8
3	74259	0.50	33.0

4	70798	0.50	31.3
5	77563	0.47	29.6
6	86674	0.45	28.0
7	62288	0.53	26.4
8	42183	0.73	24.4

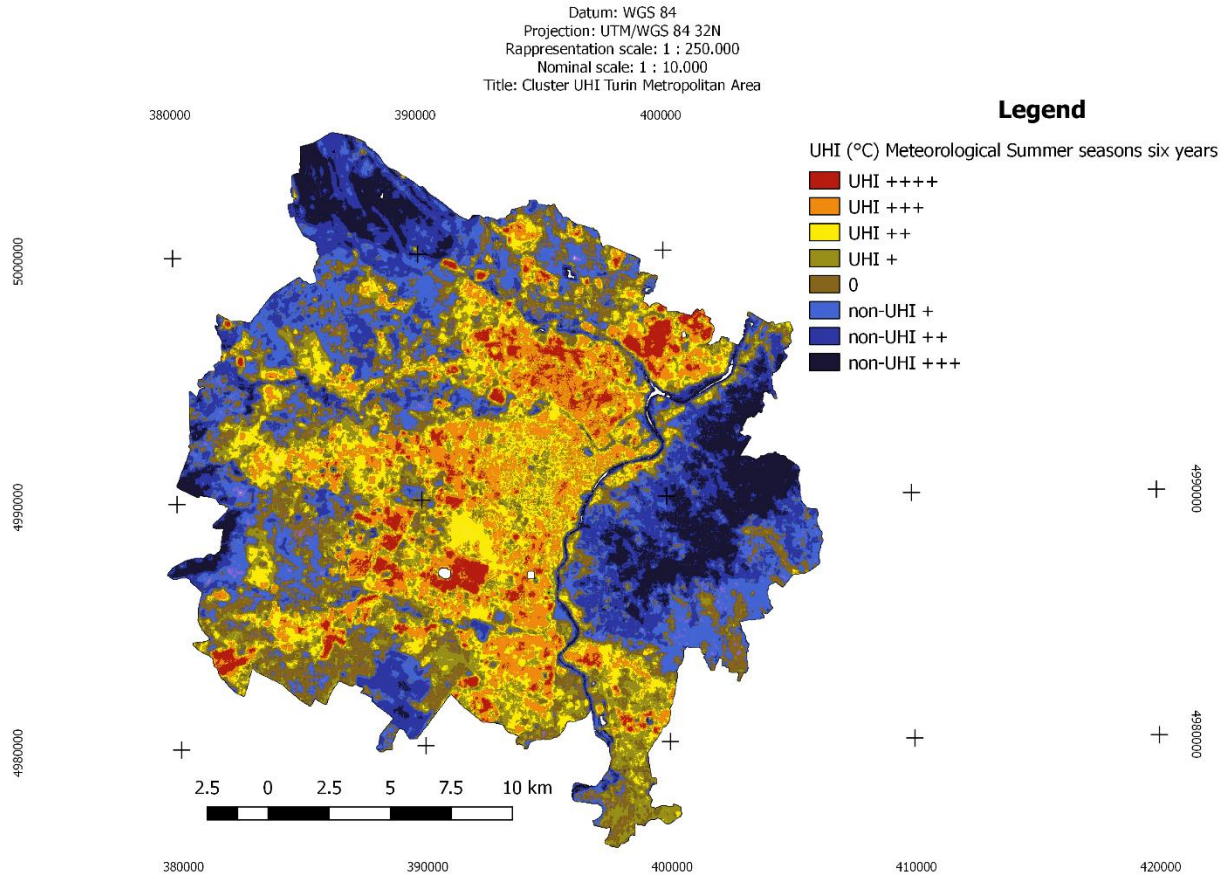

Fig.6 UHI clusters meteorological summer seasons considering six years and relative data table (Reference Frame: WGS84 UTM 32N)

UHS were more abundant in the built-up industrial areas along the northern and southern parts of Turin due to lack of both vegetation and shadows despite the higher albedo of exposed surface. Roadways, power plants, metal roofs, parking area and industrial factories are most suitable places for the development of UHS.

Cluster	Elements	Std.Dev.	UHS Mean temperature (°C) all seasons
1	29001	1.81	24.3
2	67664	1.01	20.4
3	82770	0.90	17.2
4	85111	0.88	14.1
5	88826	0.87	11.1
6	81594	0.92	8.1
7	47979	1.22	4.7
8	14096	2.71	-1.0

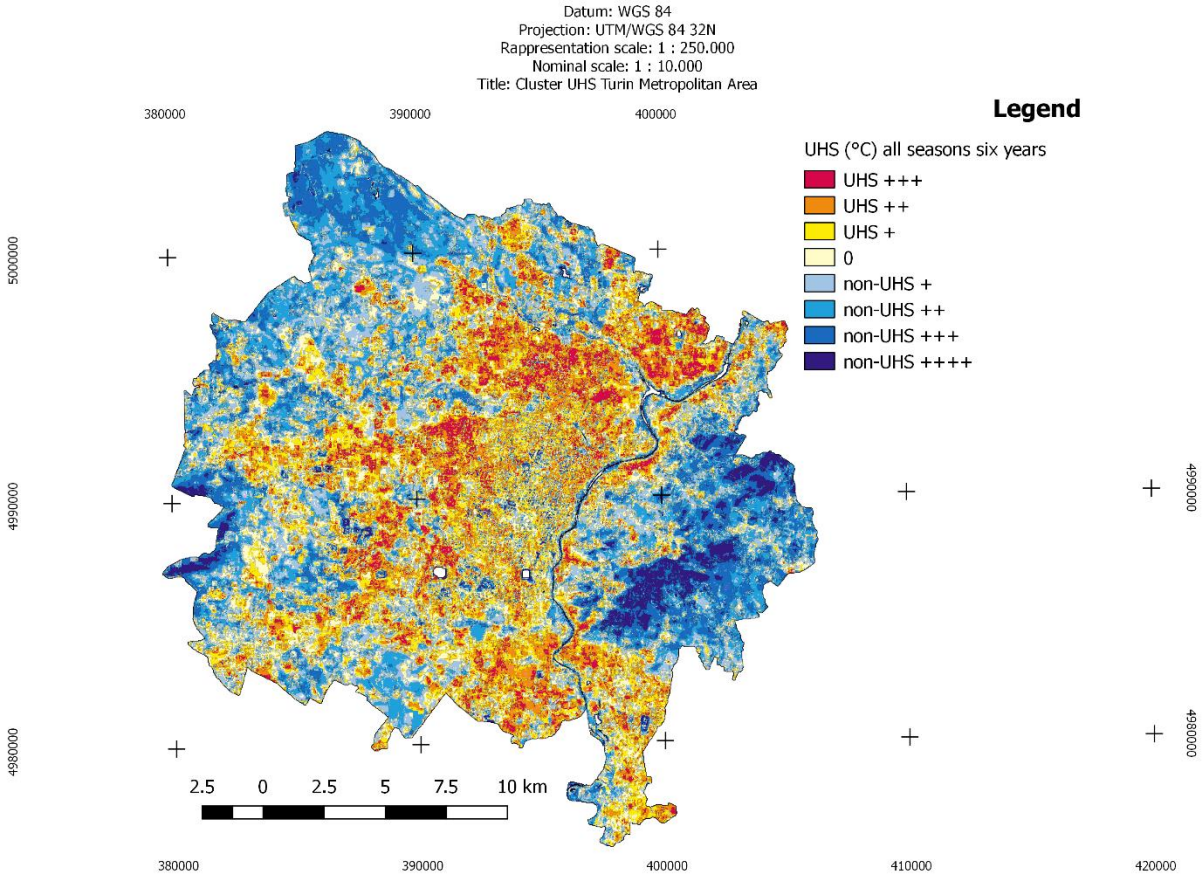

Fig.7 UHS clusters all seasons considering six years and relative data table (Reference Frame: WGS84 UTM 32N)

Cluster	Elements	Std.Dev.	UHS Mean temperature (°C) Meteorological Summer
1	34783	1.66	43.7
2	69728	1.01	39.9
3	77638	0.94	36.6
4	76698	0.94	33.4
5	83260	0.90	30.1
6	83531	0.92	27.1
7	53937	1.13	23.7
8	17466	2.09	18.9

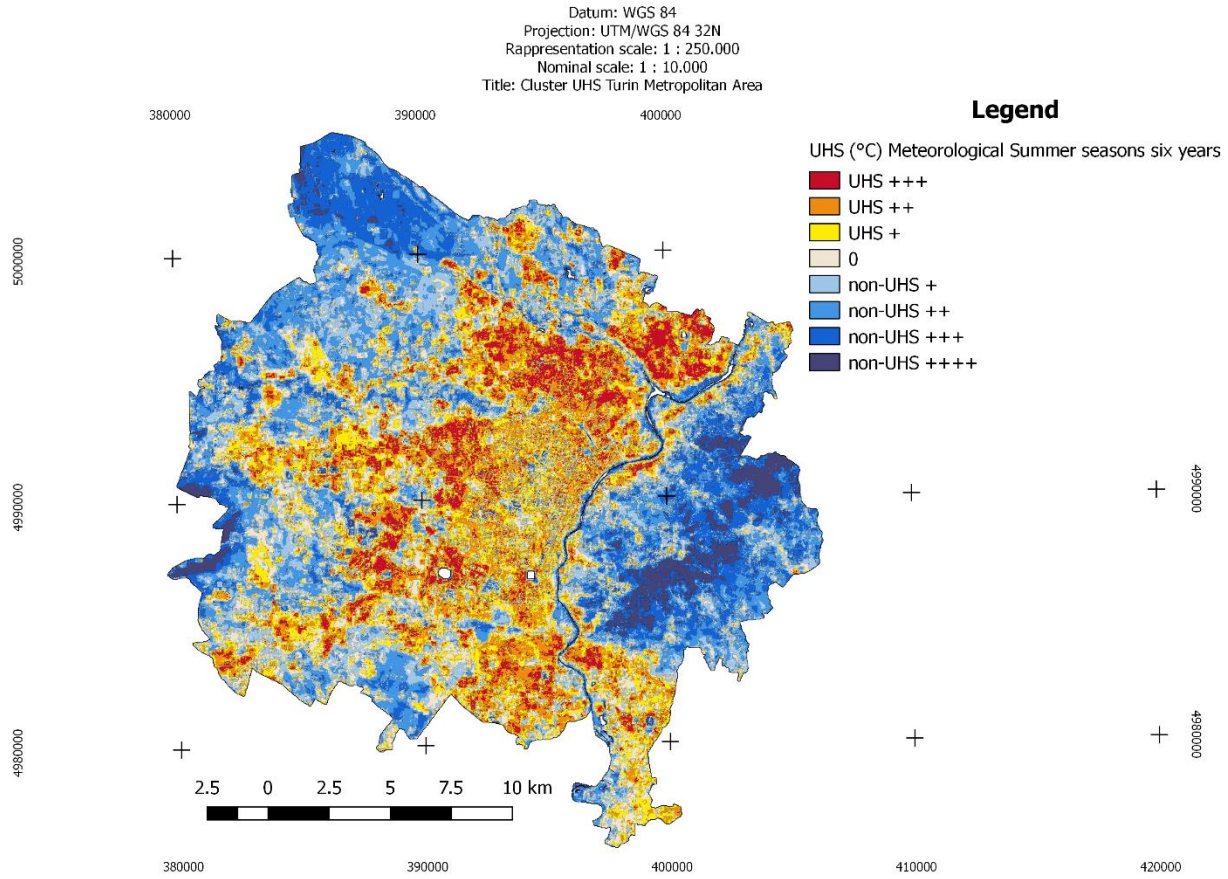

Fig.8 UHS clusters meteorological summer seasons considering six years and relative data table (Reference Frame: WGS84 UTM 32N)

Almost all hot spots have a very little or negligible amount of vegetation and water bodies. In general, LST presents a positive relationship with urban areas and an inverse relationship with NDVI. Because of this NDVI shows a strong negative correlation with LST for the whole city (−0.80) and for the non-UHI (−0.59). This strength becomes weaker for UHI (−0.41) this is due to the presence of complexity in landscape composition. Thus, LST–NDVI and LST in urban areas both build stronger correlation in large natural landscapes, while it tends to be weaker in small built-up areas.

It is very interesting fact that LST distribution is very closely related to the distribution of NDVI and Urban areas. Generally, LST is negatively related to NDVI and positively related to urban areas. But, this relationship may be varied due to spatial resolution, latitudinal extension or seasonal variation.

CONCLUSIONS

Remote sensing has many interesting new applications, especially in the last decade [52,53], in particular in this article, Landsat 8 OLI and TIRS data were used to investigate the UHI intensity effect in the metropolitan area of Turin in Italy and to interpret the dynamic relationship between LST with LC/LU (Land Use & Land Cover) through years. LST mapping has important applications [54-59]. UHI zones were identified through LST. Bare land and built-up area are mostly responsible for LST generation. The presence of vegetation and water bodies reduces the LST level so urban forestry could rapresent a useful tool in order to regulate thermal exchanges and increasing resistance and resilience against summer hate waves. Furthermore, the relationships between LST–NDVI was interpreted quantitatively by linear regression analysis at the pixel level. For whole metropolitan area of Turin, LST

shows strong negative correlation with NDVI; and strong positive correlation with anthropogenic areas (buildings, factories, etc). The relationships become weaker for UHI. It may be due to the presence of more heterogeneous landscapes within the built-up area. Also, it has to consider that Summer high temperatures and heat waves are usually matched with an increasing demand of energy for cooling in general with a tremendous impact on carbon emissions and pollution. In future, many additional research works may be included especially those in planning and manage city. Regulating energy exchanges through forestry for example evaluating how to manage smartly UHI in function of the seasons and energy consumption. Mapping UHI and LST through years may be a useful tool in health care sector. Further studies may concern how to manage humans and animals exposure to heat waves risks. In fact, the identification of areas most exposed to thermal extremes may help to well organize and manage health care resources and identifying neighborhoods with more vulnerable population. First, LST may be retrieved using another method or different spatial resolution. Second, the in situ LST data may be measured with the same overpass of satellites for the calibration and validation of LST estimation. Third, apart from linear regression, several new statistical methods can be applied to estimate the correlation between LST and different LU–LC indices. Finally, ecological evaluation of UHI zones may be analysed with the inclusion of more biophysical parameters. Last, but not least UHI can be helpful in energy management. They are useful in Winter while negative in Summer. A good strategy to regulate UHI in function of the season, it may be rapresented by planting broadleaves and study their contribute in the regulation of energy exchanges and thermal fluxes. At the present only green city and wood buildings and new materials may represent good solutions to increase resistance and resilience to heat waves and in general climate change effects in anthropic areas.

ACKNOWLEDGEMENT

A particular thanks to Gianmarco Corvino and the colleagues of the research group Geo4Agri for helping and great support during the processing phase and also a great thanks at the Department of Physics of the University of Turin (Unito) and the engineer Andrea Tartaglino Energy Manager of Unito. Last but not least ARPA Piemonte, and in particular the meteorological service for its remarkable and continuous work collecting data useful, not only for forecast predictions, but also for scientific research in many fields.

REFERENCES

[1] Chapin, F., Sturm, M., Serreze, M., McFadden, J., Key, J., Lloyd, A., McGuire, A., Rupp, T., Lynch, A., Schimel, J. “Role of Land-Surface Changes in Arctic Summer Warming,” Science 2005, 310, 657–660.

[2] Kalnay, E., Cai, M. “Impact of Urbanization and Land-use Change on Climate. Nature,” 2003, 423, 528–531.

[3] Ramanathan, V., Crutzen, P., Kiehl, J., Rosenfeld, D. “Aerosols, Climate, and the Hydrological Cycle,” Science 2001, 294, 2119–2124.

[4] Wan, Z., Wang, P., Li, X. “Using MODIS Land Surface Temperature and Normalized Difference Vegetation Index Products for Monitoring Drought in the Southern Great Plains, USA,” Int. J. Remote Sens. 2004, 25, 61–72.

[5] Gallego-Elvira, B., Taylor, C.M., Harris, P.P., Ghent, D., Veal, K.L., Folwell, S.S. “Global observational diagnosis of soil moisture control on the land surface energy balance,” Geophys. Res. Lett. 2016, 43, 2623–2631.

[6] Haffke, C., Magnusdottir, G. “Diurnal cycle of the South Pacific Convergence Zone in 30 years of satellite images,” J. Geophys. Res. Atmos. 2015, 120, 9059–9070.

[7] Zhang, X., Friedl, M.A., Schaaf, C.B., Strahler, A.H. “Climate controls on vegetation phenological patterns in northern mid- and high latitudes inferred from MODIS data,” Glob. Chang. Biol. 2004, 10, 1133–1145.

[8] Masiello, G., Serio, C., Venafra, S., Liuzzi, G., Göttsche, F., F. Trigo, I., Watts, P. “Kalman filter physical retrieval of surface emissivity and temperature from SEVIRI infrared channels: A validation and intercomparison study,” Atmos. Meas. Tech. 2015, 8, 2981–2997.

[9] Blasi, M.G., Liuzzi, G., Masiello, G., Serio, C., Telesca, V., Venafra, S. “Surface parameters from seviri observations through a kalman filter approach: Application and evaluation of the scheme to the southern Italy,” Tethys 2016, 2016, 1–19.

[10] Weng, Q. “Thermal infrared remote sensing for urban climate and environmental studies: Methods, applications, and trends,” ISPRS J. Photogramm. Remote Sens. 2009, 64, 335–344.

[11] Kalma, J., McVicar, T., McCabe, M. “Estimating Land Surface Evaporation: A Review of Methods Using Remotely Sensed Surface Temperature Data,” Surv. Geophys. 2008, 29, 421–469.

[12] Anderson, M.C., Allen, R.G., Morse, A., Kustas, W.P. “Use of Landsat thermal imagery in monitoring evapotranspiration and managing water resources. Remote Sens,” Environ. 2012, 122, 50–65.

[13] Wang, K., Dickinson, R.E. “A review of global terrestrial evapotranspiration: Observation, modeling, climatology, and climatic variability”, Rev. Geophys. 2012, 50.

[14] Jha, S.K., Mariethoz, G., Evans, J.P., McCabe, M.F. “Demonstration of a geostatistical approach to physically consistent downscaling of climate modeling simulations,” Water Resour. Res. 2013, 49, 245–259.

[15] Hengl, T., Heuvelink, G.B.M., Perˇcec Tadi´c, M., Pebesma, E.J. “Spatio-temporal prediction of daily temperatures using time-series of MODIS LST images,” Theor. Appl. Climatol. 2012, 107, 265–277.

[16] Yu, X., Guo, X., & Wu, Z. “Land Surface Temperature Retrieval from Landsat 8 TIRS—Comparison between Radiative Transfer EquationBased Method, Split Window Algorithm and Single Channel Method,” Remote Sensing, 6(10), 2014, 9829-9852.

[17] Kleerekoper, L., van Esch, M., Salcedo, T.B., “How to make a city climate-proof, addressing the urban heat island effect,” Resour. Conserv. Recycl. 2012, 64, 30–38.

[18] Nakayama, T., Hashimoto, S., “Analysis of the ability of water resources to reduce the urban heat island in the Tokyo megalopolis,” Environ. Pollut. 2011, 159, 2164–2173.

[19] Emmanuel, R., Krüger, E. “Urban heat island and its impact on climate change resilience in a shrinking city: The case of Glasgow, UK,” Build. Environ. 2012, 53, 137–149.

[20] Li, W., Wang, Y., Peng, J., Li, G. “Landscape spatial changes associated with rapid urbanization in Shenzhen, China,” Int. J. Sustain. Dev. World Ecol. 2005, 12, 314–325.

[21] Wong, J.K.W., Lau, L.S.-K. “From the ‘urban heat island’ to the ‘green island’? A preliminary investigation into the potential of retrofitting green roofs in Mongkok district of Hong Kong,” Habitat Int. 2013, 39, 25–35.

[22] Kukla, G., Gavin, J., Karl, T., “Urban warming”, J. Appl. Meteorol. 1986, 25, 1265–1270.

[23] Tomlinson, C.J., Chapman, L., Thornes, J.E., Baker, C.J. “Derivation of Birmingham’s summer surface urban heat island from MODIS satellite images,” Int. J. Climatol. 2012, 32, 214–224.

[24] Rao, P.K. “Remote Sensing of Urban Heat Islands from an Environmental Satellite,” Bull. Am. Meteorol. Soc. 1972, 53, 647–648.

[25] Pan, J. “Area Delineation and Spatial-Temporal Dynamics of Urban Heat Island in Lanzhou City, China Using Remote Sensing Imagery”, J. Indian Soc. Remote Sens. 2015, 44, 111–127.

[26] Howard, L., “The Climate of London Deduced from Meteorological Observations Made in the Metropolis and at Various Places around It,”, Harvey and Darton: London, UK, 1833, Volume 1, p. 348.

[27] Zinzi, M. “Cool materials and cool roofs: Potentialities in Mediterranean buildings,”Adv. Build. Energy Res. 2010, 4, 201–266.

[28] Weng, Q., Yang, S. “Managing the adverse thermal effects of urban development in a densely populated Chinese city,” J. Environ. Manag. 2004, 70, 145–156.

[29] Rinner, C., Hussain, M. Toronto’s Urban Heat Island—Exploring the Relationship between Land Use and Surface Temperature. Remote Sens. 2011, 3, 1251–1265.

[30] Georgescu, M., Moustaoui, M., Mahalov, A., Dudhia, J. “An alternative explanation of the semiarid urban area “oasis effect,”Journal of Geophysical Research, 116, 2011, D24113.

[31] Du, S., Xiong, Z., Wang, Y., & Guo, L. “Quantifying the multilevel effects of landscape composition and configuration on land surface temperature,” Remote Sensing of Environment, 2016, 178, 84–92

[32] Song, J., Du, S., Feng, X., & Guo, L. “The relationships between landscape compositions and land surface temperature: Quantifying their resolution sensitivity with spatial regression models. Landscape and Urban Planning,” 2014, 123, 145–157.

[33] Asgarian, A., Amiri, B.J., & Sakieh, Y., “Assessing the effect of green cover spatial patterns on urban land surface temperature using landscape metrics approach,”, Urban Ecosystems, 2015, 18, 209–222.

[34] Arnfield, A.J., “Two decades of urban climate research: a review of turbulence, exchange of energy and water, and the urban heat island”, Int. J. of Climatology, 2002, 23, 1–26

[35] Weng, Q. “Thermal infrared remote sensing for urban climate and environmental studies: Methods, applications, and trends,” ISPRS J. Photogramm. Remote Sens. 2009, 64, 335–344.

[36] Jiménez-Muñoz, Juan C., and José A. Sobrino. "A generalized single-channel method for retrieving land surface temperature from remote sensing data," Journal of Geophysical Research: Atmospheres 108.D22 (2003).

[37] Lopez, Juan Miguel Rodriguez, Katharina Heider, and Jürgen Scheffran. "Frontiers of urbanization: identifying and explaining urbanization hot spots in the south of Mexico City using human and remote sensing," Applied geography 79 (2017): 1-10.

[38] Deilami, Kaveh, and Md Kamruzzaman. "Modelling the urban heat island effect of smart growth policy scenarios in Brisbane," Land Use Policy 64 (2017): 38-55.

[39] Fratianni, Simona, and Fiorella Acquaotta. "The climate of Italy," *Landscapes and Landforms of Italy*. Springer, Cham, 2017. 29-38.

[40] Gorelick, N., Hancher, M., Dixon, M., Ilyushchenko, S., Thau, D., & Moore, R. “Google Earth Engine: Planetary-scale geospatial analysis for everyone,” Remote Sensing of Environment 2017.

[41] Conrad, O., Bechtel, B., Bock, M., Dietrich, H., Fischer, E., Gerlitz, L., Wehberg, J., Wichmann, V., and Boehner, J. “System for Automated Geoscientific Analyses (SAGA) v. 2.1.4,” Geosci. Model Dev., 2015, 8, 1991-2007, doi:10.5194/gmd-8-1991-2015.

[42] Markham, Brian, et al. "Landsat-8 operational land imager radiometric calibration and stability," Remote Sensing 6.12, 2014, 12275-12308.

[43] QGIS Development Team. "QGIS geographic information system," Open Source Geospatial Foundation Project, Versão 2.7 (2015).

[44] Sobrino, José A., Juan C. Jimenez-Munoz, and L. Paolini. "Land surface temperature retrieval from LANDSAT TM 5," *Remote Sensing of environment* 90.4 (2004): 434-440.

[45] Sobrino, J. A., N. Raissouni, and Zhao-Liang Li. "A comparative study of land surface emissivity retrieval from NOAA data," *Remote Sensing of Environment* 75.2 (2001): 256-266.

[46] Jimenez-Munoz, J. C., Sobrino, J., Skokovic, D., Mattar, C., & Cristobal, J. (2014). Land surface temperature retrieval methods from Landsat-8 thermal infrared sensor data. Geoscience and Remote Sensing Letters, IEEE, 11(10), 2003, 1840-1843.

[47] Skoković, D., Sobrino, J. A., Jimenez-Munoz, J. C., Soria, G., Juşien, Y., Mattar, C., & Cristóbal, J. “Calibration and validation of land surface temperature for landsat8-tirs sensor” LPVE (Land Product Validation and Evolution 2014.

[48] Carlson, Toby N., and David A. Ripley. "On the relation between NDVI, fractional vegetation cover, and leaf area index," *Remote sensing of Environment* 62.3 (1997): 241-252.

[49] Weng, Qihao, Dengsheng Lu, and Jacquelyn Schubring. "Estimation of land surface temperature–vegetation abundance relationship for urban heat island studies," *Remote sensing of Environment* 89.4 (2004): 467-483.

[50] O'Connor, Amanda, et al. "ENVI Services Engine: Earth and planetary image processing for the cloud," *American Geophysical Union, Poster IN21C-1490* (2012).

[51] Guha, Subhanil, Himanshu Govil, and Sandip Mukherjee. "Dynamic analysis and ecological evaluation of urban heat islands in Raipur city, India," Journal of Applied Remote Sensing 11.3 (2017): 036020.

[52] Borgogno-Mondino, E., Sarvia, F., & Gomarasca, M. A., "Supporting Insurance Strategies in Agriculture by Remote Sensing: A Possible Approach at Regional Level," In International Conference on Computational Science and Its Applications (2019, July), (pp. 186-199). Springer, Cham.

[53] De Petris, S., Boccardo, P., & Borgogno-Mondino, E., "Detection and characterization of oil palm plantations through MODIS EVI time series," International Journal of Remote Sensing, (2019), 40(19), 7297-7311.

[54] Barsi, Julia A., Schott, John R., Hook, Simon J., Raqueno, Nina G., Markham, Brian L., Radocinski, Robert G., "Landsat-8 Thermal Infrared Sensor (TIRS) Vicarious Radiometric Calibration" Remote Sens., no. 11: 6, 2014, 11607-11626.

[55] Chander, G., & Markham, B. "Revised Landsat-5 TM radiometric calibration procedures and postcalibration dynamic ranges," Geoscience and Remote Sensing, IEEE Transactions on, 41(11), 2674-2677.

[56] Cristóbal, J., Ninyerola, M., Pons, X. "Modeling air temperature through a combination of remote sensing and GIS data," J. Geophys. Res. 2008, 113.

[57] U.S.Geological Survey Landsat 8 (l8) data users handbook, Version 1.0, June, 2015. online: http://landsat.usgs.gov/documents/Landsat8DataUsersHandbook.pdf

[58] Voogt, J. A., & Oke, T. R. "Thermal remote sensing of urban climates," Remote sensing of environment, 86(3), 370-384.

[59] Yu, X., Guo, X., & Wu, Z. "Land Surface Temperature Retrieval from Landsat 8 TIRS—Comparison between Radiative Transfer EquationBased Method, Split Window Algorithm and Single Channel Method," Remote Sensing, 6(10), 2014, 9829-9852.